ESC499 Thesis Interim Report

Feedback Guidance Laws for Planetocentric Orbital Maneuvering of Solar Sail Spacecraft by Lyapunov Methods

Interim Progress Report

Mingde Yin

University of Toronto

Supervised by Professor Christopher Damaren

University of Toronto Institute for Aerospace Studies

January 19, 2024

Contents

List of Figures

List of Tables

Chapter 1

Introduction

This chapter presents introductory context for the project, and frames the scope of the project around key challenges associated with targeted maneuvering of solar sail spacecraft in planetocentric orbits.

1.1 Scope

This project aims to develop a guidance law for performing planetocentric orbital transfers with a solar sail spacecraft, using a simplified feedback approach derived from Lyapunov control theory.

The goal of the guidance law is to achieve acceptable values for time-of-flight while requiring a minimal set of considerations for spacecraft configuration.

Convergence and time optimality of the guidance law are considered, but are not rigorously assessed or proven. Instead, these characteristics are assessed through simulations spanning a variety of initial/target orbits and spacecraft configurations.

An extended study is conducted to tune the parameters of the guidance law for minimum time-of-flight.

1.2 Motivation

Low-thrust spacecraft have been the focus of spacecraft guidance research in recent decades, paving the way for the dominance of low-thrust trajectories in contemporary space missions. Electric propulsion has attained widespread adoption [1, 2], while solar sails have remained

obscure [3]. Developing practical solar sailing guidance laws is a critical precursor for the acceptance of solar sails as a useful propulsion method.

Earth orbit remains the most prolific destination for space missions, and there exist many proposed applications of solar sailing in this domain. Existing literature is largely focused on specific problems, including orbit raising [4], Earth escape [5], and end-of-life deorbiting [6]. A more general problem of maneuvering solar sail spacecraft between two arbitrary orbits around a planet is considered for this project, as it has received limited study.

1.3 Key Challenges and Gap

Planetocentric orbital maneuvering of solar sail spacecraft poses two significant challenges compared to conventional spacecraft.

1. Solar sails produce little thrust [7], making classical impulse-based orbital maneuvering theory unsuitable for trajectory planning. Low-thrust trajectory planning for planetocentric orbits is itself a challenging domain of study; traditional approaches using collocation struggle with the "winding" nature of consecutive orbits.

2. Thrust is dependent on the orientation of the spacecraft relative to incoming sunlight. Thrust availability depends on the direction of incident light, which cannot be directly controlled. For example, a solar sail cannot produce thrust directly towards incoming sunlight, akin to a sailboat sailing directly into the wind. Furthermore, real solar sails are typically limited in terms of how much they can be misaligned from incident sunlight, owing to both thrust production and attitude control needs [7].

Low-thrust planetocentric orbital maneuvering has been approached using methods derived from feedback control theory [8–11]. Instead of approaching trajectory guidance as a global optimization problem, feedback guidance laws trade global optimality for better convergence behaviour and simplicity. This class of guidance laws has been explored in the context of solar sailing, but formulated with an assumed form of relationship between sail thrust and orientation relative to the Sun. Notably, a recent guidance law developed by Oguri (2023) [12] depends on 3 parameters representing the contributions of different modes of light reflection.

A key appeal of feedback guidance laws is their relative independence from system parameters. It is therefore appealing to consider a solar sailing guidance law which is agnostic to the parameters of the solar sail. Such a guidance law would facilitate trajectory analysis for unique and esoteric spacecraft designs, and remain applicable as better reflectivity models for solar sails are developed.

1.4 Implementation

The guidance law is implemented as a two-stage algorithm, combining a solution obtained from conventional low-thrust feedback guidance theory with an additional set of adaptations to make the solution amenable to solar sails.

The first stage is based on a control-Lyapunov function, Q, in a formulation called the *Q-Law* first introduced by Petroupolos (2004) [9]. A reformulation presented by Varga and Pérez (2016) [10] using analytical approximations to the derivatives of Q is used to produce a desired sail orientation based on a spacecraft state in modified equinoctial orbital elements. The intermediate guidance solution is regularized to obey constraints associated with the alignment of the sail relative to incoming sunlight.

A computer model of the guidance law is tested in simulations. A MATLAB implementation is used for high-fidelity simulations and performance validation. A lower-fidelity but faster implementation in C is used to optimize the parameters of the guidance law for minimum time-of-flight.

Chapter 2

Background

This chapter presents a expands on the background covered in the introduction, discussing specific topics driving the approach taken to solving the problem. The literature review is divided into four sections:

1. Spacecraft trajectory guidance at large, for which solar sail guidance is a subset;
2. Feedback guidance laws, particularly the *Q-Law* derived from Lyapunov control theory;
3. Special considerations needed for solar sails beyond conventional low-thrust spacecraft;
4. Approaches to solar sail guidance, particularly planetocentric orbital maneuvering.

2.1 Spacecraft Trajectory Guidance at Large

This section covers essential aspects of spacecraft orbits, followed by a discussion of various approaches used to develop guidance laws for orbital maneuvering. Techniques for low-thrust spacecraft are given focus, as those are most relevant to solar sails.

2.1.1 The Planetocentric Guidance Problem

The general problem of planetocentric orbital maneuvering refers to altering the orbit of a spacecraft around a parent celestial body from some initial orbit to a final target orbit. (Note that this is different from *rendezvous*, which adds a further constraint that the spacecraft must reach a certain point along the target orbit at a specific time, i.e. to meet with a spacecraft already in that target orbit.)

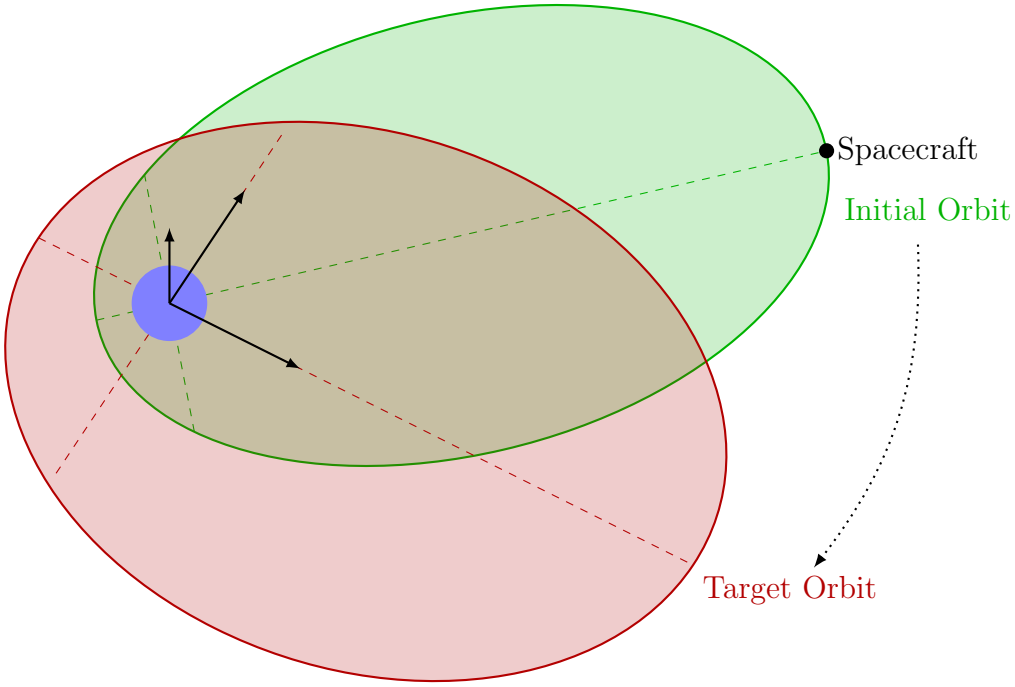

Figure 2.1: Cartoon illustration of the planetocentric orbital maneuvering guidance problem.

Solving the guidance problem refers to generating a sequence of applied thrust vectors which modify the spacecraft's orbit accordingly. Since the solution is generally not unique, the space of all valid guidance solutions can be searched for those which result in the shortest time of flight or the least propellant expenditure, for example. Hence, the guidance problem is often considered approached as an optimization problem [13].

2.1.2 Description and Evolution of Spacecraft Orbits

Orbits (in the context of the two-body problem) are described using a set of 6 orbital elements [14]. Keplerian orbital elements are the most prolific, but there exist alternative formulations of two-body spacecraft orbits which also result in 5 elements specifying orbital geometry/orientation and 1 element representing time.

Some examples:

- Keplerian Elements $\{a, e, i, \Omega, \omega, \theta\}$
- Modified Equinoctial Elements $\{p, f, g, h, k, L\}$ [15]
- Gooding Universal Elements $\{\alpha, q, i, \Omega, \omega, \tau\}$ [16]

Altering the orbit of a spacecraft to solve the guidance problem involves changing its orbital elements. The process of solving for the evolution of orbital elements in time is known as *orbit propagation*.

Cowell's method [14] is a well-known way of propagating general spacecraft trajectories in Cartesian state space. Typically this involves integrating equations of motion derived from Newton's second law in a form similar to the following:

$$\frac{\mathrm{d}^2\boldsymbol{r}}{\mathrm{d}t^2} = -\frac{\mu}{||\boldsymbol{r}||^3}\boldsymbol{r} + \boldsymbol{f}_p \tag{2.1}$$

Wherein $\boldsymbol{f}_p$ is some perturbing acceleration (i.e. unrelated to point-mass gravity of the central body) and $\boldsymbol{r}$ is the position vector of the spacecraft (both expressed in an inertial frame). Although simple at first glance, a difficulty of working in Cartesian coordinates for spacecraft guidance is that all six values of the state vector (position and velocity) change in time, regardless of the presence of perturbations. Additionally, describing the geometry of an orbit in terms of Cartesian state is not as straightforward as using orbital elements.

Variational Methods for Orbit Propagation

Variational equations of motion are ordinary differential equations giving the time derivatives of orbital elements when subject to a perturbing acceleration, such as thrust from a propulsion system. Taking Keplerian elements as an example, they take the form:

$$\frac{\mathrm{d}}{\mathrm{d}t}\begin{bmatrix} a \\ e \\ i \\ \Omega \\ \omega \\ \theta \end{bmatrix} = A\boldsymbol{f}_p + \boldsymbol{b}$$

Where $A \in \mathbb{R}^{6\times6}$, $\boldsymbol{b} \in \mathbb{R}^{6\times6}$, and typically only the last entry of $\boldsymbol{b}$ is nonzero (i.e. the other 5 orbital elements are invariant when there is zero perturbing acceleration).

When posed in terms of variational equations of motion, the guidance problem becomes one of determining the perturbing acceleration needed at each instant in time to **change the orbital elements of the spacecraft which describe the geometry and orientation of the orbit** (e.g. in the case of Keplerian elements, a, e, i, Ω, ω).

Compared to Cowell's method, working directly in terms of orbital elements dramatically simplifies the analysis of guidance laws, particularly in discussing convergence to the target orbit.

Comparison with Classical Orbital Maneuvering Theory

Classical orbital maneuvering theory employs brief, high-thrust maneuvers which are approximated as impulses, leading to a sequence of discrete orbits constituting a maneuver, and removing the need to analyze trajectories in terms of continuous equations of motion. Impulse-based maneuvering theory has been extensively studied and is commonly taught at the undergraduate level, as demonstrated by books such as Ref. [14]. On the other hand, low-thrust guidance requires time integration of differential equations, making the majority of analysis **heavily-reliant on numerical simulation**. One common approach used for solving the guidance problem for a (low-thrust) solar sail spacecraft is to **integrate the variational equations of motion**.

2.1.3 The Case for Modified Equinoctial Elements

The 5 Keplerian elements describing the geometry and orientation of an orbit are the semi-major axis (a), eccentricity (e), inclination (i), right ascension of the ascending node (Ω), and argument of periapsis (ω). The remaining orbital element used to represent time is the true anomaly (θ). A significant challenge associated with using Keplerian elements and their respective variational equations in trajectory analysis are the **singularities** which occur for many types of orbits (e.g. circular orbits, zero-inclination orbits). Although no orbits are perfectly circular or zero-inclination in practice, the singularities appearing in both the orbital elements themselves and their associated variational equations cause numerical issues in simulations.

Common solutions to this include adding "deadbands" to the values of eccentricity and inclination, such when they are decremented under some threshold (e.g. $|e| < 10^{-4}$), their value is clamped to the lower bound until their rates of change become positive. This is the approach taken by Petropoulos (2004) [9] to avoid reaching singularities.

Modified equinoctial orbital elements defined by Walker et. al (1985) [15] remove singularities in all cases except for a perfectly retrograde equatorial orbit, and present many numerical conveniences for analysis. They are defined from Keplerian elements as follows:

$$
\begin{aligned}
p &= a(1-e^2) & h &= \tan(i/2)\cos\Omega \\
f &= e\cos(\omega+\Omega) & k &= \tan(i/2)\sin\Omega \\
g &= e\sin(\omega+\Omega) & L &= \Omega+\omega+\theta
\end{aligned}
$$

In contrast to Keplerian elements, the modified equinoctial elements (f, g, h, k) describing the orientation of the orbit represent ratios instead of angles, and are order unity (when

$i \in [-90°, 90°]$). Perfectly circular and equatorial orbits are handled without issues in the variational equations of motion (shown later in Equation 3.3).

The heavy dependence of numerical simulation for the analysis low-thrust spacecraft trajectories makes modified equinoctial elements a good basis for developing a guidance law.

2.1.4 Global Optimization Methods for Low-Thrust Trajectories

One common approach used for low-thrust trajectory planning is posing the guidance problem as a global optimization problem. At a high level, there exists two main classes of methods: direct and indirect methods, along with variants thereof. These are presented in depth in a survey of the state of the art by Morante et al. (2021) [17], but the essential points are discussed here. Note that global methods often employ a Cartesian state formulation instead of orbital elements.

Both methods construct a sequence (i.e. a time history) of control inputs which bring the spacecraft to a targeted state. Both methods also discretize the problem by assuming a certain form for the control inputs (e.g. piecewise polynomials). Direct methods solve for unknown coefficients using pseudospectral or other collocation-based methods through integration of the equations of motion and direct evaluation of the functional to be optimized. Indirect methods (also referred to as adjoint, co-state, or primer vector methods) use the calculus of variations and Lagrangian multipliers to produce systems of equations with sufficient constraints for optimality which are then solved to get the unknown coefficients. As described by Kelly (2015) in an introductory overview paper of global optimization [18], direct methods find coefficients to minimize a functional, while indirect methods solve a system of equations which "set the gradient of the functional to be zero".

For interplanetary missions, the timescale of the astrodynamics (i.e. the period of orbits around the Sun) is similar to the timescale of the optimization problem (i.e. the time of flight), making the problem computationally tractable through use of a coarse discretization. The Sims-Flanagan method, a direct method, is highly amenable for interplanetary trajectories [13, 19]. Collocation-based methods (e.g. Gauss pseudospectral methods) are used in similar applications [20, 21].

A critical weakness of global optimization approaches for trajectory planning is their dependence on an initial guess. Indirect methods in particular struggle with stably converging to a solution when presented with a poor initial guess. For simple interplanetary trajectories, intuition is sufficient to kickstart an optimization, but the complex nature of orbital transfers around a planet is considerably less intuitive.

As discussed in the introduction, a challenging aspect of planetocentric orbital maneuvering is the mismatch in timescales between orbital periods and time of flight. Referred to as **multirevolution transfers**, trajectories making a large number of revolutions around a planet require a very fine mesh to accurately capture the "curvature" of the orbits. An extremely low-thrust propulsion system such as a solar sail may need hundreds of revolutions to raise its orbit, increasing computational complexity considerably.

Consequently, this project focuses on an entirely different approach to spacecraft guidance – locally optimal feedback guidance.

2.2 Feedback Guidance Laws

Classical control theory is built upon the idea of simple feedback control loops. Although designed without any guarantees for global optimality, they are simple to implement, and can be tuned to get near-optimal performance.

The same idea has been applied to guidance in two main forms: thrust-blending and Lyapunov control. Both approaches use formulations using orbital elements for state representation. In both cases, the key idea is to take the difference between the current value and target value for each orbital element, and produce a control input which decreases the error at each timestep.

Thrust-blending (also referred to as blended control) methods find control inputs which independently maximize the rate of decrease of the error for each of the orbital elements, and take a linear combination of the individual inputs. This is examined more thoroughly in the survey by Morante et al. (2021) [17].

Lyapunov methods take an alternative approach compared to thrust-blending, by instead maximizing the rate of decrease of an error function, comprised of the errors in each orbital element.

2.2.1 Lyapunov Methods

A brief primer on Lyapunov control theory is presented, based on an explanation from the fundamental paper of planetocentric Lyapunov-based guidance by Ilgen (1994) [8].

Consider a dynamic system with state $x(t) \in \mathbb{R}^n$ a control input $u \in \mathbb{R}^m$ governed by some differential equation $f : \mathbb{R}^n \times \mathbb{R}^m \to \mathbb{R}^n$ s.t. $\dot{x}(t) = f(x(t), u)$.

Consider a function $V : \mathbb{R}^n \to \mathbb{R}$, called a **potential function or control-Lyapunov**

function, which maps each state value to some scalar. Intuitively, this can be thought of as analogous to the potential energy of the system, which vanishes at some point $x = \hat{x}$, e.g. a mass attached to a spring, wherein $V(x) = \frac{1}{2}(x - \hat{x})^2$

This dynamic system is said to be **Lyapunov stable** iff a potential function can be found which meets the following conditions:

1. $V(x) > 0 \; \forall \; x \neq \hat{x}$
2. $V(\hat{x}) = 0$
3. There exists some u for all $x \in \mathbb{R}^n$ s.t.

$$\dot{V} = \nabla V(x) \cdot \dot{x}(t) = \nabla V(x) \cdot f(x, u) < 0$$

Where $\nabla V(x)$ means $\dfrac{\mathrm{d}V}{\mathrm{d}x_i} = \left\{ \dfrac{\mathrm{d}V}{\mathrm{d}x_1}, ..., \dfrac{\mathrm{d}V}{\mathrm{d}x_n} \right\}$

Or in other words:

- $V(x)$ is positive definite
- For every state, there exists a control input which decreases $V(x)$ in time.

Over time, this will drive the state towards $x = \hat{x}$.

This is a powerful idea, because it can be used both as a means to prove the stability of a system, and also as a means of developing a feedback control law $u = u(x, t)$

Solving for the value of u at each value of x such that $\dot{V}$ is minimized produces a **locally optimal feedback control law**.

2.2.2 Early Control-Lyapunov Functions

Ilgen's paper proposes a potential function which is a linear combination of the square of the difference between each orbital element and its target value. Formulated in Keplerian elements, it is given as:

$$V = \frac{1}{2}\left[P_1 \frac{(a - \hat{a})^2}{R_e^2} + P_2(e - \hat{e})^2 + P_3(i - \hat{i})^2 + P_4(\Omega - \hat{\Omega}) + P_5(\omega - \hat{\omega})^2\right] \tag{2.2}$$

where hatted values refer to target orbital elements, and $P_i, i \in 1, ..., 5$ are weighting factors.

At each timestep, the only thing needed to compute the control input is the current state of the spacecraft – there is **no dependence on past or future states**, making the guidance law extremely cheap computationally.

Additionally, given the relatively simple nature of the potential function, it is possible to derive analytical expressions for the control input. However, given that Ilgen's potential function is expressed in Keplerian elements, there are singularities in the derivatives of V.

Nonetheless, Ilgen demonstrates **nearly time-optimal behaviour** from this guidance law, making it a competitive alternative to global methods.

Importantly, Ilgen demonstrates guaranteed convergence to the final target orbit under certain limiting conditions. This is remarkable, as **no knowledge of the global solution is needed** to converge to the target orbit. However, a complete analysis of convergence in the general case is not given.

This paper highlights many of the key strengths and weaknesses of Lyapunov methods for guidance. While Lyapunov methods are simple to implement, cheap to simulate, and performant, it is challenging to rigorously analyze the performance of feedback guidance laws, particularly with regards to convergence guarantees and convergence rate. The lack of coupling to the global solution makes it difficult to robustly ascertain that a locally optimal solution can be extended to the global domain.

Another example of a control-Lyapunov guidance law is demonstrated by Naasz [22].

A notable contemporary development in Lyapunov-based planetocentric orbit maneuvering guidance is a family of guidance laws spawned from the *Q-Law*.

2.2.3 The Q-Law Family

The *Q-Law* was developed by Petropoulos [9] using a potential function of the form:

$$Q = (1 + W_P P) \sum_{\text{œ}} W_{\text{œ}} S_{\text{œ}} \left(\frac{\text{œ} - \hat{\text{œ}}}{\dot{\text{œ}}_{\max}} \right)^2 \quad \text{œ} \in \{a, e, i, \Omega, \omega\} \tag{2.3}$$

where P is a penalty function used to impose constraints, $S_{\text{œ}}$ is a scaling function for each orbital element, and $W_\sigma, \sigma \in \{P, a, e, i, \Omega, \omega\}$ are weights. $\hat{\text{œ}}$ represents target orbital elements, and $\dot{\text{œ}}_{\max}$ represents the maximum attainable rate of change in each orbital element across the course of an orbit (i.e. across all values of θ) and across all thrust directions (assuming a propulsion system with fixed thrust).

Q is described as a "proximity quotient"; each term in the summation can be thought of as the square of the minimum time needed to drive the error in a single orbital element to zero.

One of the key brilliancies of the approach is implementing a means to compensate for **how "easy" it is to change a given orbital element** (through $\dot{\text{œ}}_{\max}$). Orbital elements which

have a lower possible maximum rate of change are weighed with more importance by the potential function. This mechanism allows for the error in each orbital element to "balance out" over time, which is important for practically ensuring stability and convergence.

$\dot{oe}_{max}$ can be computed from the variational equations of motion, and results in an analytical expression for the derivatives of Q. Note that when formulated in modified equinoctial elements, analytical approximations are used for $\dot{oe}_{max}$ [10, 11].

Petropoulos' original paper has been built upon numerous times for different applications, including rendezvous [11]. Varga and Pérez (2016) [10] give an implementation in modified equinoctial elements, along with a study on optimizing the values of $W_\sigma, \sigma \in \{P, a, e, i, \Omega, \omega\}$.

The *Q-Law* family has demonstrated remarkably good performance when subjected to higher fidelity studies, incorporating eclipse effects (i.e. rendering electric propulsion inoperable when occluded from sunlight), and J2 perturbation [10]. Although solar sails are a relatively fresh application for this type of guidance law, the long history of good performance under challenging conditions shows promise for this project.

2.3 Considerations for Solar Sails

Solar sails are a propulsion method requiring no propellant expenditure to produce thrust. The principle of operation is based on conservation of momentum in the reflection of incident photons from the Sun. Challenges associated with performing controlled maneuvers using solar sails are described, with discussions of implications on spacecraft guidance. Fundamental principles are taken with reference to McInnes (1999) [7].

The most challenging aspects of bringing solar sails into reality are not actually related to trajectory planning; truthfully, the greatest issues lie in the manufacturing and production of solar sails; material science and mechanical design remain the greatest barriers to the widespread adoption of solar sails [7]. On top of that, attitude control is a fundamental precursor to thrust control, and is still in a highly development stage [23].

With that said, an important fact to consider is that real solar sails behave very differently from an ideal flat sail. As discussed by Polyakhova (2018) in a review of solar sailing missions, models describing the thrust produced by solar sails continue to change with every new spacecraft built and flown [24].

In a perfectly idealized model, thrust is produced exactly in the direction of the sail normal, and the cone angle can be as great as 90°. Real solar sails have limits on maximum allowable

cone angle due to considerations for attitude control or because the reflective material of the sail behaves non-ideally at shallow incidence angles. Furthermore, the resultant thrust vector is not always aligned perfectly with the sail normal. This is illustrated in Figure 2.2 below.

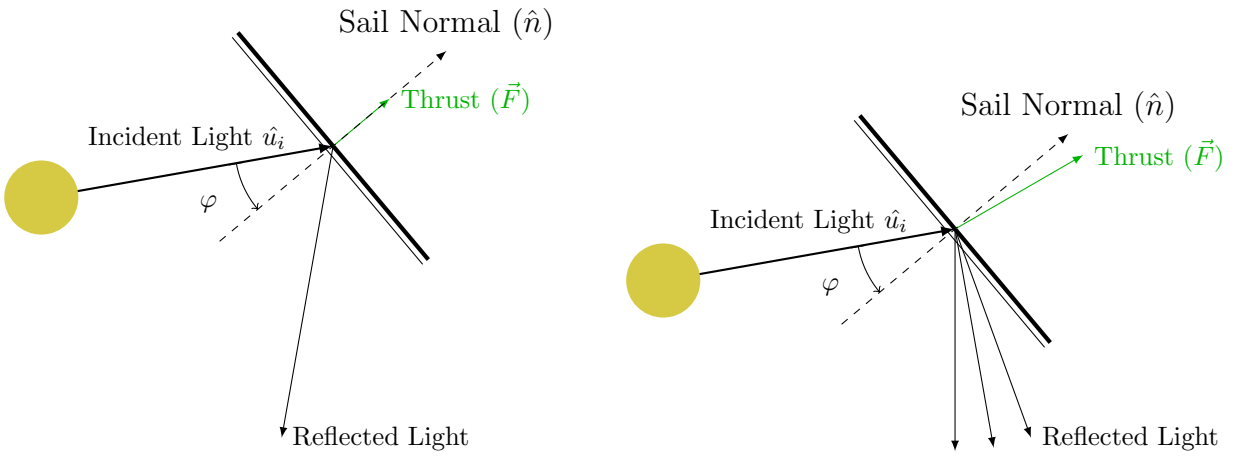

(a) Perfectly reflecting sail, where the thrust vector is aligned with the sail normal.

(b) General sail, which may scatter and absorb incoming light, resulting in offset thrust.

Figure 2.2: Differences between a general reflectivity model and a perfectly reflecting sail.

2.3.1 Inherent Challenges of Dynamics

Even in the case of a flat perfectly reflecting sail, there are two key obstacles complicating the application of low-thrust guidance theory to solar sail spacecraft.

1. **Direction-Dependent Availability of Thrust**: The thrust produced by a solar sail is related to the cone angle φ by a factor of roughly $\cos^2(\varphi)$ (see Equation 2.22 of Ref. [7]). Thrust falls off considerably as the sail becomes misaligned with the direction of incident light, and drops to zero for $|\varphi| > 90°$. This means that at any instant in time, only a single hemisphere of thrust directions can be realized, with the orientation of the hemisphere being dependent on the position of the Sun – a quantity which cannot be directly controlled. This is illustrated in Figure 2.3a.

2. **Time/Position-Dependent Availability of Thrust**: In addition to the limitations on the direction in which thrust can be produced, the availability of thrust itself depends on a clear line of sight to the Sun. In eclipse, no light hits the sail, and no thrust is produced. This is illustrated in Figure 2.3b. For spacecraft in low orbits above a planet, the time spent in eclipse represents a substantial fraction of the orbital period, and exacerbates the challenge of maneuvering using a solar sail.

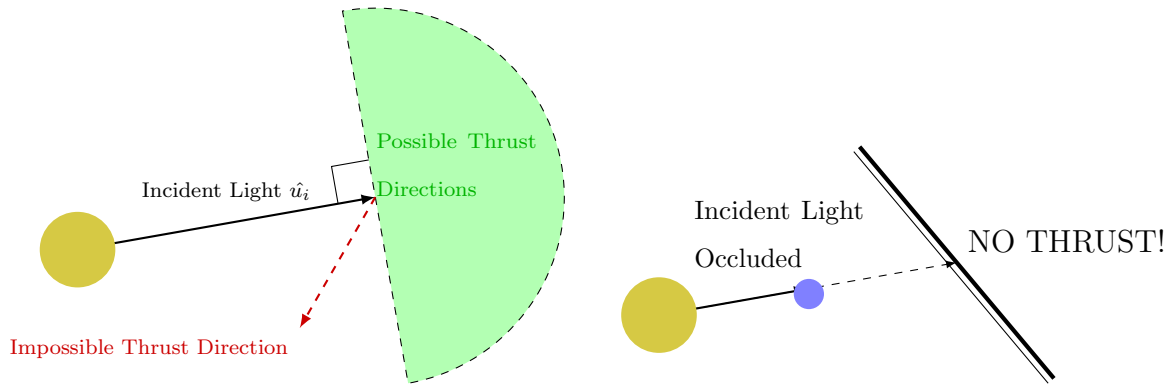

(a) The direction of produced thrust is limited for a (flat perfectly reflecting) solar sail.

(b) Solar sails produce no thrust in eclipse.

Figure 2.3: Key challenges associated with solar sail thrust.

Both of these effects are present to a lesser degree in spacecraft using electric propulsion; solar arrays require Sun exposure, but are typically made to rotate so that they can track the Sun independently of the direction of the engines. Solar sails pose a more extreme set of challenges for maneuvering, stemming from their principle of operation.

2.3.2 Diversity of Sail Geometries and Materials

McInnes (1999) [7] discusses several different solar sail geometries and reflectivity models with considerably different forms.

Real solar sails do not adhere to perfectly flat geometries due to deformation effects [25], and can even be designed intentionally with non-flat geometry for enhanced attitude control capabilities [26].

IKAROS (2010) featured variable-reflectivity materials on its surface for attitude control [27], and sail materials are an ongoing field of development, as discussed in a review of the state of the art by NASA (2011) [28].

The key point to be made is that fixating upon a certain dynamic model for solar sails is overly restrictive for adequate consideration of future solar sail designs.

Note that there is work done by Rios-Reyes et al. (2005) [29] and Tsunda et al. (2013) [30] on generalizing solar sail dynamics models. These models allow for arbitrary geometries and surface reflectivity properties, but have a large number of parameters. For the sake of simplicity, integrating such a model into the guidance law for this project is not considered.

2.4 Solar Sail Guidance

As with low-thrust guidance, solar sails have frequently been the subject for interplanetary (heliocentric) trajectories. Analytical analysis of inward and outward spiral trajectories around the Sun are discussed by McInnes (1999) [7]. However, the focus of this literature review is on planetocentric orbital maneuvering.

In planetocentric orbits, the issues of directional thrust availability and eclipse are more severe than when around the Sun. For instance, the "hemisphere" of allowable thrust directions (see Figure 2.3a) makes a full revolution during each orbit around the Sun, and therefore a solar sail in heliocentric orbit can apply thrust in nearly all directions over the course of a single orbit. On the other hand, the position of the Sun relative to a spacecraft barely changes over the course of a single orbit around a planet, which greatly restricts the possible space of thrust directions. As already mentioned, eclipse is a common occurrence in low orbit around a planet, while it is effectively nonexistent when orbiting the Sun.

2.4.1 Specialized Guidance Laws for Planetocentric Orbital Maneuvers

As discussed by Polyakhova (2018) [24], there are numerous applications of solar sails in Earth orbit, including orbit raising, de-orbiting, and sending spacecraft onto escape trajectories. For each of these applications, a specialized guidance law can be developed.

Coverstone and Prussing (2003) [5] present a feedback guidance law for escaping Earth from a geosynchronous transfer orbit. The technique employed is most similar to thrust-blending guidance laws, in which the rate of change of orbital energy is maximized. This guidance law performs to within the correct order of magnitude (in terms of time of flight) for a minimum-time escape, and demonstrates the utility of feedback guidance laws in planetocentric orbits. This guidance law performs a very specific task of sending a spacecraft onto an escape trajectory, solving the guidance problem for a special case of final orbit.

Fieseler (1998) [4] discusses a scheme for orbit raising with simply applies thrust along the velocity vector of the solar sail. This is taken as the core of a design featuring angled flaps to direct thrust in a prograde direction without incurring excessive atmospheric drag in low Earth orbit. This guidance scheme does not allow for targeting of a specific orbit, and a more sophisticated guidance law would need to be used once the orbit is raised to a point where drag is negligible.

2.4.2 Generalized Orbital Maneuvering

The overall field of planetocentric orbital maneuvering using solar sails is much less studied than the general low-thrust case. There are few examples of guidance laws for maneuvering between arbitrary orbits around a planet.

One of the oldest approaches to this problem is presented by Sackett (1977) [31], using an indirect global optimization approach. This work produced examples of both orbit-to-orbit transfers, as well as escape trajectories. A key concern with the results from this work was the generation of unrealistic trajectories which flew very close to or into the Earth's surface.

MacDonald and McInnes (2005) [32] were among the first to formulate a contemporary feedback guidance law for orbital maneuvering. Their approach was to use a feedback guidance law using thrust-blending. This was the first use of a penalty function to prevent the spacecraft from plunging into the Earth.

The most recent development in the field is a paper from Oguri (2023) [12], which adapts the *Q-Law* for use with solar sails, by incorporating a popular sail reflectivity model into the guidance law (done by incorporating sail thrust into the $\dot{\alpha e}_{\max}$ terms of Q). This work demonstrated that the remarkable performance of the *Q-Law* could be readily transferred to solar sails given adequate consideration for solar sail dynamics.

2.5 Research Gap and Approach

Given the robustness of the *Q-Law* to disturbances in environment and dynamics, it is interesting to consider an approach similar to that taken by Oguri (2023) [12], except without needing to incorporate solar sail dynamics directly into the derivatives of Q.

The ingredients for such an approach are already well-established, and the prospect of demonstrating good performance of a guidance law with a more general form appears feasible.

The choice of a Lyapunov-based feedback guidance law is supported by a healthy lineage of research in low-thrust spacecraft guidance, and the inclination to keep the guidance law as general as possible is motivated by the ongoing evolution of solar sail spacecraft designs and dynamics models.

Chapter 3

Problem Formulation and Implementation

The formulation of the guidance law is presented in this chapter, along with an overview of its implementation in numerical simulation.

3.1 Problem Definition and Assumptions

The objective of this project is to develop a feedback guidance law for transferring between two orbits around a planet in orbit around the Sun using a solar sail spacecraft.

Stated more formally, the problem is given as:

Planetocentric Solar Sail Feedback Guidance Problem
Consider a spacecraft propelled by an ideal flat solar sail with sail loading σ and efficiency η in an ideal 2-body orbit around a planet with gravitaional parameter μ (which itself orbits the Sun). Let be P the radiation pressure of incident sunlight, which comes from a known direction $\hat{u}_i$.
Given the instantaneous spacecraft state $\{p, f, g, h, k, L\}$ and target orbit described by the elements $\{\hat{p}, \hat{f}, \hat{g}, \hat{h}, \hat{k}\}$, determine an instantaneous spacecraft orientation in the LVLH frame (i.e. the sail normal $\hat{n}$, presented in the form of steering angles α and β) which ultimately brings the spacecraft to the target orbit.

The terms of this statement are elaborated in the proceeding subsections.

3.1.1 Orbit and Environment

The spacecraft is assumed to be orbiting a planet, possessing an instantaneous state expressed in modified equinoctial elements (p, f, g, h, k, L) (i.e an osculating orbit). The spacecraft is targeting an orbit described in modified equinoctial elements, as $\{\hat{p}, \hat{f}, \hat{g}, \hat{h}, \hat{k}\}$

The position of the spacecraft with respect to the planet is given by the vector $\vec{r}$, and the absolute velocity of the spacecraft is given by $\vec{v}$.

Remark on Notation: Mathematical notation for vectors follows the vectrix convention, as used in Ref. [14]. Abstract vectorial quantities are written with the arrow above (e,g $\vec{u}$), and vectors expressed in a reference frame $\vec{\mathcal{F}}$ are written in boldface (e.g. $\boldsymbol{u}$). Unit vectors are given a special notation, written using a hat (e.g. $\hat{u}$).

Reference Frames

Two reference frames are used in this problem, defined in Table 3.1, based on common convention. The frame $\vec{\mathcal{F}}_I$ has its origin at the center of the planet, and is taken to be inertial. The $\vec{\mathcal{F}}_{\text{LVLH}}$ is attached to the spacecraft, and its orientation is defined by the position vector of the spacecraft and the plane of the orbit.

Frame Name	Symbol	x-direction	y-direction	z-direction
Inertial	$\vec{\mathcal{F}}_I$	Points in direction of Υ	Perpendicular to $\hat{x}_I$ in equatorial plane	$\hat{z}_I = \hat{x}_I \times \hat{y}_I$
LVLH	$\vec{\mathcal{F}}_{\text{LVLH}}$	$\frac{\vec{r}}{\|\|\vec{r}\|\|}$	$\frac{\vec{r}\times\vec{v}\times\vec{r}}{\|\|\vec{r}\times\vec{v}\times\vec{r}\|\|}$	$\frac{\vec{r}\times\vec{v}}{\|\|\vec{r}\times\vec{v}\|\|}$

Table 3.1: The frames involved, and their definitions.

Quantities related to the guidance law are expressed in the LVLH frame, including steering command outputs. This choice of frame is motivated by past formulations of the *Q-Law*, which are based on variational equations in the LVLH frame.

Sun

The Sun is located at a position $\vec{r}_\odot$ with respect to the planet, and hence the vector going from the Sun to the spacecraft is given by $\vec{r} - \vec{r}_\odot$. The direction of incident light is therefore given by $\hat{u} = -\frac{\vec{r}-\vec{r}_\odot}{\|\|\vec{r}-\vec{r}_\odot\|\|}$.

A diagram describing the elements of the problem discussed so far is shown in Figure 3.1.

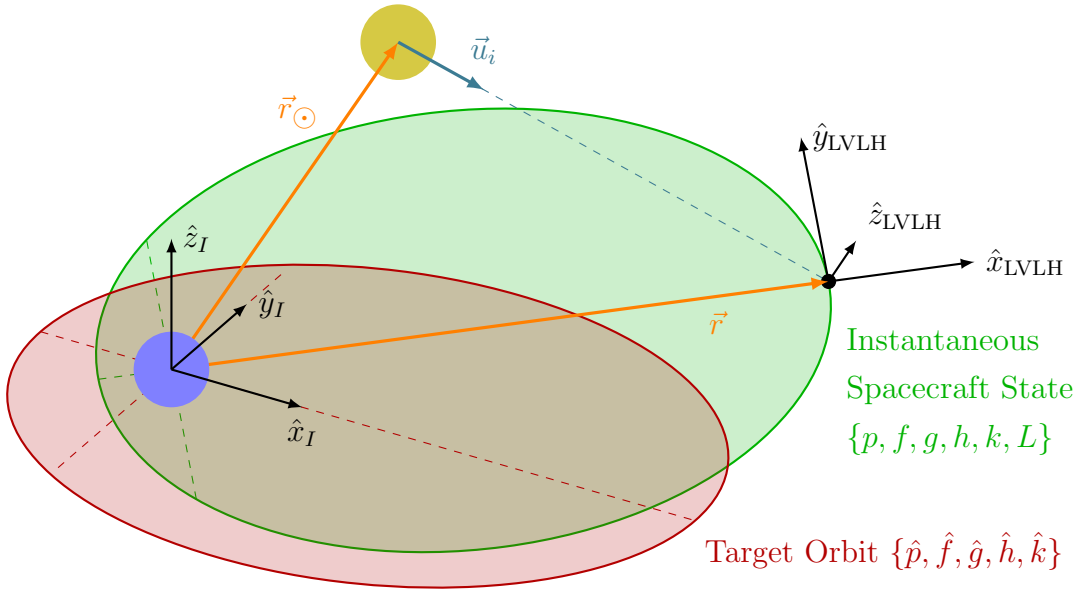

(a) Spatial setup of problem, primary view.

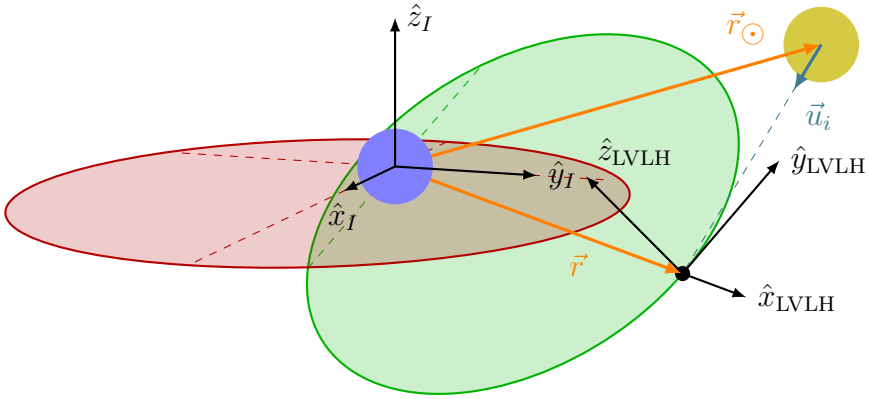

(b) Spatial setup of problem, alternate view.

Figure 3.1: Diagram of key elements of the problem (multiple views for clarity). The planet is represented by the blue circle, the Sun by the yellow circle, and the spacecraft by the black dot.

3.1.2 Spacecraft Orientation Convention

The output of the guidance law is a spacecraft orientation in the LVLH frame. That is, the guidance law expresses the unit vector $\hat{n}$ in terms of the output steering angles α and β.

The convention used in this project follows Refs. [9–11], and is depicted in Figure 3.2.

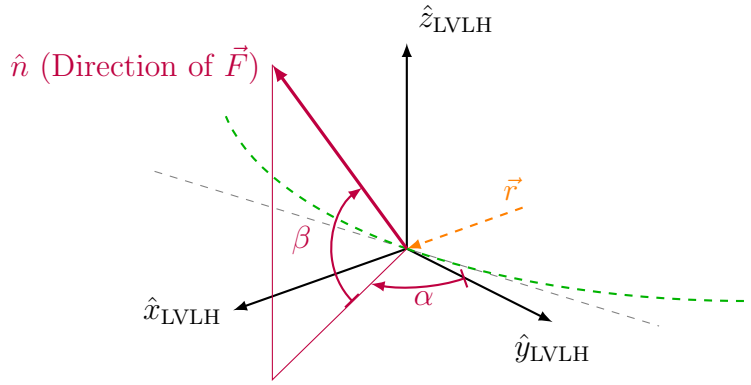

Figure 3.2: Thrust angle orientation convention. Note that generally, $\alpha = 0$ does NOT correspond to the direction of the velocity vector of the spacecraft, as $\vec{\mathcal{F}}_{\text{LVLH}}$ is aligned with $\vec{r}$ and $\vec{r} \times \vec{v}$. The dashed grey line represents the tangent line to the orbit, which is generally not aligned with $\hat{y}_{\text{LVLH}}$.

α is a clockwise steering angle from the y-axis in the xy LVLH plane, and β is a steering angle towards the $+z$ axis.

That is to say, the direction vector of the spacecraft is given by:

$$\hat{n}(\alpha, \beta) = \vec{\mathcal{F}}^{T}_{\text{LVLH}} \begin{bmatrix} \cos\beta \sin\alpha \\ \cos\beta \cos\alpha \\ \sin\beta \end{bmatrix} \tag{3.1}$$

3.1.3 Dynamics

Sail Thrust

Dynamics for an idealized flat solar sail are presented and used in the implementation of numerical simulations.

For a solar sail pointing in the direction $\hat{n}$ and for incident light in the direction $\hat{u}_i$, the acceleration imparted on the sail is given by:

$$\vec{F} = \frac{2P\eta}{\sigma}(\hat{u}_i \cdot \hat{n})^2 \text{sign}(\hat{u}_i \cdot \hat{n})\hat{n} \ [\text{ms}^{-2}] \tag{3.2}$$

Where $P = 9.12 \times 10^{-6}\,\text{Nm}^{-2}$ is the value of solar radiation pressure at a distance of 1 AU. The quantity $\sigma = \frac{m}{A}$ $[\text{kgm}^{-2}]$ referred to as *sail loading* is the mass of the spacecraft divided by the sail area, and is conventionally used to parameterize sail performance. A dimensionless efficiency factor η represents "how reflective" the material of the sail is, relative

to a perfect reflector. The leading coefficient of 2 results from force imparted both by incident and reflected photons.

Variational Equations of Motion

The equations of motion of the spacecraft are given by (3.3) below.

$$\frac{\mathrm{d}}{\mathrm{d}t}\begin{bmatrix} p \\ f \\ g \\ h \\ k \\ L \end{bmatrix} = \frac{1}{q}\sqrt{\frac{p}{\mu}}\begin{bmatrix} 0 & 2p & 0 \\ q\sin L & (q+1)\cos L + f & -g(h\sin L - k\cos L) \\ -q\cos L & (q+1)\sin L + g & f(h\sin L - k\cos L) \\ 0 & 0 & \frac{\cos L}{2}(1+h^2+k^2) \\ 0 & 0 & \frac{\sin L}{2}(1+h^2+k^2) \\ 0 & 0 & h\sin L - k\cos L \end{bmatrix}\begin{bmatrix} F_r \\ F_\theta \\ F_n \end{bmatrix} + \begin{bmatrix} 0 \\ 0 \\ 0 \\ 0 \\ 0 \\ \frac{q^2\sqrt{\mu p}}{p^2} \end{bmatrix} \tag{3.3}$$

$$\text{with} \quad q \equiv 1 + f\cos L + g\sin L$$

F_r, F_θ, F_n correspond to perturbing accelerations on the spacecraft expressed in the LVLH frame corresponding to the radial, tangential, and normal directions respectively. That is:

$$\vec{F} = \vec{\mathcal{F}}^T_{\text{LVLH}}\begin{bmatrix} F_r \\ F_\theta \\ F_n \end{bmatrix}$$

3.1.4 Motion of the Sun

The sun is assumed to be 1.5×10^8 m from the center of the coordinate system, at an angle varying by 2π in 1 year ($\tau = 365.25\,\mathrm{d} = 31\,557\,600\,\mathrm{s}$).

That is,

$$\vec{r}_\odot(t) = 1.5 \times 10^8 \ \vec{\mathcal{F}}^T_I \begin{bmatrix} \cos(\lambda_\odot) \\ \sin(\lambda_\odot)\cos(\varepsilon) \\ \sin(\lambda_\odot)\sin(\varepsilon) \end{bmatrix} \mathrm{m} \tag{3.4}$$

Where $\lambda_\odot = \frac{2\pi}{\tau}t$, with $t = 0$ corresponding to the vernal equinox, and $\varepsilon = 23.439°$ is the obliquity of the ecliptic.

This is obviously not reflective of Earth's elliptical orbit around the Sun, but it is assumed to be adequate as a starting point.

In this analysis, the position of the Sun is considered to be **quasi-static**, that is, $\dot{\lambda}_\odot = 0$, since the motion of the Sun occurs on a timescale much longer than the period of an orbit.

3.2 Methodology

The guidance law is implemented in a two-stage architecture, depicted in Figure 3.3 below. The guidance law occupies the left half of the diagram (blocks in blue and green), while the rest of the dynamics are shown in the purple blocks on the right.

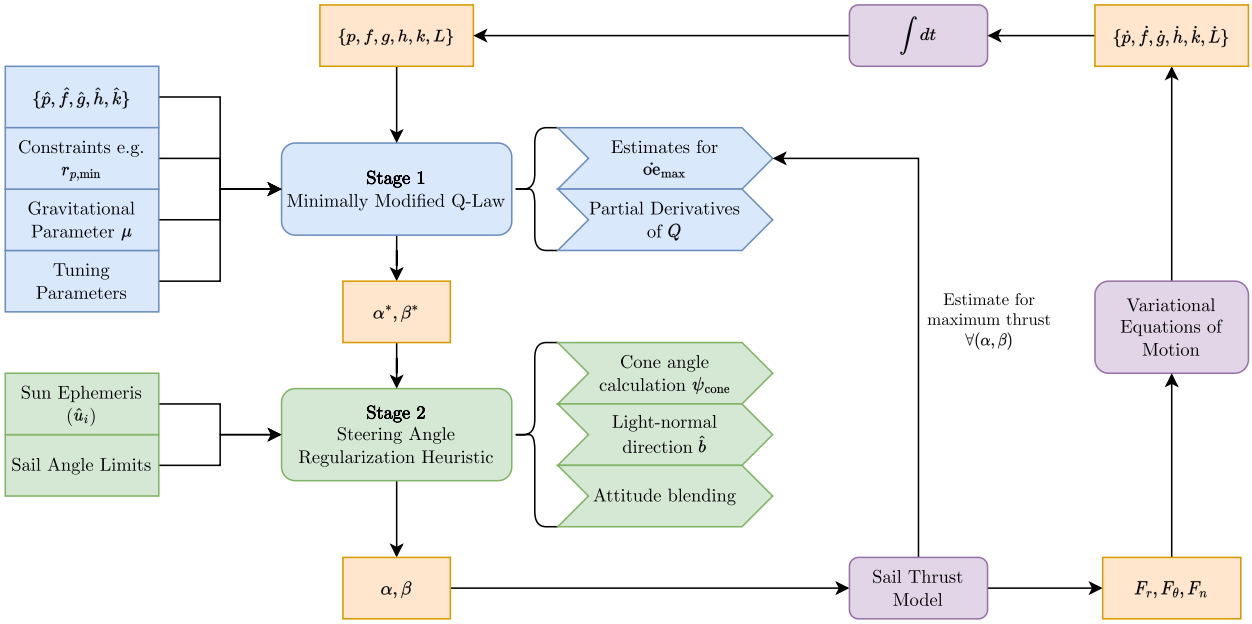

Figure 3.3: Architecture of the guidance law, along with the dynamics of the spacecraft.

The key idea is to consider all solar sail-related elements (direction of incident light, restrictions on orientation) independently of the formulation for the "idealized" steering angles. The first stage of the guidance law treats the solar sail as if it were a regular low-thrust spacecraft capable of producing an acceleration $F_{\max}$ at constant thrust. From this, it generates idealized angles α^*, β^*, which are then regularized by the second stage to make them feasible for a solar sail to use.

Rather than try to rework the *Q-Law*, the heuristic attached to the original guidance law transforms the solar sail guidance problem into a more conventional low-thrust guidance problem with modified dynamics. That is, the steering angle regularization block can be thought of as being part of the dynamics, with the *Q-Law* operating as if it were controlling a regular low-thrust spacecraft.

3.3 Formulation of Minimally Modified Q-Law

The minimally modified *Q-Law* is derived in this section, along with a computational procedure for assembling the steering angle outputs.

3.3.1 Control-Lyapunov Function

The minimally modified *Q-Law* is structured very similarly to previous works (Refs. [9–11]), following a control-Lyapunov function Q, which is then differentiated in terms of steering angles α, β to determine the direction maximizing $-\dot{Q}$.

The control-Lyapunov function is given below in Equation 3.5.

$$Q = (1 + W_P P) \sum_{\text{œ}} W_{\text{œ}} S_{\text{œ}} \left(\frac{\text{œ} - \hat{\text{œ}}}{\dot{\text{œ}}_{\max[\alpha,\beta,L]}} \right)^2 \quad \text{œ} \in \{p, f, g, h, k\} \tag{3.5}$$

$$S_{\text{œ}} = \begin{cases} \frac{1}{R_e} & \text{œ} = p \\ 1 & \text{Otherwise} \end{cases}$$

$$P = \exp\left[\gamma \left(1 - \frac{r_p}{r_{p,\min}} \right) \right]$$

$$a = \frac{p}{1 - e^2}$$

$$r_p = a(1 - e) = p\frac{(1 - e)}{(1 + e)(1 - e)} = \frac{p}{1 + \sqrt{f^2 + g^2}}$$

with $\dot{\text{œ}}_{\max[\alpha,\beta,L]}$ being taken to mean the maximum achieveable rate of change in that orbital element for any value of steering angles (α, β) and true longitude L.

The only variables in Q are $\text{œ} \in \{p, f, g, h, k\}$, and therefore Q can be written as a sum of derivatives using the chain rule:

$$\dot{Q} = \sum_{\text{œ}} \frac{\partial Q}{\partial \text{œ}} \dot{\text{œ}}$$

Note that Equation 3.3 in fact gives $\dot{\text{œ}}$ as a function of F_r, F_θ, F_n. The idea then is to link $\dot{Q}$ to the thrust model for the solar sail, without being overly specific. The key assumption taken for deriving the *Q-Law* portion of the guidance law is to **assume that the solar sail always produces its maximum possible thrust in any direction**. Hence, Equation 3.6 is taken to be true for the purposes of deriving ideal steering angles.

$$\begin{bmatrix} F_r \\ F_\theta \\ F_n \end{bmatrix} = \frac{2P\eta}{\sigma} \begin{bmatrix} \cos\beta \sin\alpha \\ \cos\beta \cos\alpha \\ \sin\beta \end{bmatrix} \equiv F_{\max} \begin{bmatrix} \cos\beta \sin\alpha \\ \cos\beta \cos\alpha \\ \sin\beta \end{bmatrix} \tag{3.6}$$

Keeping the relationship simple using only $F_{\max}$ allows for a very general application of the guidance law to a broad range of spacecraft configurations.

3.3.2 Ideal Steering Angles

By simultaneously considering Equations 3.3 and 3.6, $\dot{\text{oe}}$ becomes a function of α and β.

$\dot{Q}$ can therefore be expressed in a form based on steering angles, shown below:

$$\dot{Q} = D_1 \cos\beta \sin\alpha + D_2 \cos\beta \cos\alpha + D_3 \sin\beta \tag{3.7}$$

For some D_1, D_2, D_3 based on other variables/parameters. Finding the stationary point of $\dot{Q}$ with respect to (α, β) gives:

$$\alpha^* = \text{atan2}\left(-D_1, -D_2\right) \tag{3.8}$$

$$\beta^* = \text{atan2}\left(-D_3, \sqrt{D_1^2 + D_2^2}\right) \tag{3.9}$$

which maximizes $-\dot{Q}$. This form is obtained from Ref. [10], where the definition of D_1 and D_2 are swapped compared to this project. The reasoning behind the ordering here is such that D_1, D_2, D_3 line up with F_r, F_θ, F_n.

3.3.3 Assembling the Guidance Output

The remaining piece consists of deriving expressions for all of the terms in Q and $\dot{Q}$ and assembling them to produce optimal steering angles.

Expressions for $\dot{\text{oe}}_{\max[\alpha,\beta,L]}$

$\dot{f}_{\max[\alpha,\beta,L]}$ and $\dot{g}_{\max[\alpha,\beta,L]}$ are taken as approximate analytical forms, first developed by Ref. [10]. The other 3 orbital elements have exact analytical expressions for maximum rate of change, obtained by manipulating Equation 3.3.

$$\dot{p}_{\max[\alpha,\beta,L]} = \frac{2p}{q}\sqrt{\frac{p}{\mu}}F_{\max}$$

$$\dot{f}_{\max[\alpha,\beta,L]} \approx 2F_{\max}\sqrt{\frac{p}{\mu}}$$

$$\dot{g}_{\max[\alpha,\beta,L]} \approx 2F_{\max}\sqrt{\frac{p}{\mu}}$$

$$\dot{h}_{\max[\alpha,\beta,L]} = \tfrac{1}{2}F_{\max}\sqrt{\frac{p}{\mu}}\frac{1+h^2+k^2}{\sqrt{1-g^2}+f}$$

$$\dot{k}_{\max[\alpha,\beta,L]} = \tfrac{1}{2}F_{\max}\sqrt{\frac{p}{\mu}}\frac{1+h^2+k^2}{\sqrt{1-f^2}+g}$$

Partials of Q

Each partial derivative of Q can be written as:

$$\frac{\partial Q}{\partial \text{œ}} = W_{\text{œ}} S_{\text{œ}} \left[W_P \frac{\partial P}{\partial \text{œ}} \left(\frac{\text{œ} - \hat{\text{œ}}}{\dot{\text{œ}}_{\max[\alpha,\beta,L]}} \right)^2 + 2(1 + W_P P) \left(\frac{\text{œ} - \hat{\text{œ}}}{\dot{\text{œ}}_{\max[\alpha,\beta,L]}} \right) \right] \quad \text{œ} \in \{p, f, g, h, k\}$$

The final forms of D_1, D_2, D_3 can now be computed from this, with a few shorthands introduced for convenience:

$$\begin{aligned}
\boldsymbol{\Xi}_E &= \left[2 \left(\frac{\text{œ} - \hat{\text{œ}}}{\dot{\text{œ}}_{\max[\alpha,\beta,L]}} \right) \right]_{\text{œ} \in \{p,f,g,h,k\}} \in \mathbb{R}^5 \\
\boldsymbol{\Xi}_P &= \left[W_P \frac{\partial P}{\partial \text{œ}} \left(\frac{\text{œ} - \hat{\text{œ}}}{\dot{\text{œ}}_{\max[\alpha,\beta,L]}} \right)^2 \right]_{\text{œ} \in \{p,f,g,h,k\}} \in \mathbb{R}^5 \\
W &= \operatorname{diag}\left(\left[W_{\text{œ}} \right]_{\text{œ} \in \{p,f,g,h,k\}} \right) \in \mathbb{R}^{5 \times 5} \\
S &= \operatorname{diag}\left(\left[S_{\text{œ}} \right]_{\text{œ} \in \{p,f,g,h,k\}} \right) \in \mathbb{R}^{5 \times 5} \\
A &= \begin{bmatrix} 0 & 2p & 0 \\ q \sin L & (q+1)\cos L + f & -g(h \sin L - k \cos L) \\ -q \cos L & (q+1)\sin L + g & f(h \sin L - k \cos L) \\ 0 & 0 & \frac{\cos L}{2}(1 + h^2 + k^2) \\ 0 & 0 & \frac{\sin L}{2}(1 + h^2 + k^2) \end{bmatrix} \in \mathbb{R}^{5 \times 3}
\end{aligned}$$

(q is defined in Equation 3.3).

$$\boldsymbol{D} = \begin{bmatrix} D_1 \\ D_2 \\ D_3 \end{bmatrix} \in \mathbb{R}^3$$

Combining everything together gives:

$$\boldsymbol{D} = \begin{bmatrix} D_1 \\ D_2 \\ D_3 \end{bmatrix} = A^T W S \left(W_P \boldsymbol{\Xi}_P + (1 + W_P P) \boldsymbol{\Xi}_E \right) \tag{3.10}$$

Combined with Equations 3.8 and 3.9, this gives a computational procedure for the ideal steering angles.

Note that $\dfrac{\partial P}{\partial \text{œ}}$ is calculated using symbolic algebra, and the expressions are omitted here because they are very ugly. It should be noted that $\dfrac{\partial P}{\partial \text{œ}}$ is nonzero only for $\text{œ} \in \{p, f, g\}$.

3.4 Steering Angle Regularization Heuristic

The steering angle heuristic is formulated in this section, beginning from a conceptual motivation of the idea.

3.4.1 Concept

If the cone angle produced by the ideal steering angles from the first stage is outside the achievable range of the solar sail, there are two options:

1. **Feather the sail**: Orient the solar sail (normal) at exactly 90° relative to the incident sunlight to produce zero thrust.
2. **Make a Compromise**: Find the "closest" valid sail orientation, subject to the cone angle restriction. (This notion of "closeness" is elaborated upon in the formulation).

Feathering the sail is useful for situations where the cone angle suggested by the first stage exceeds 90° (i.e. the sail cannot produce thrust in that direction). This prevents the spacecraft from regressing **away** from its target orbit.

The latter option is particularly helpful even in the case of an ideal flat solar sail, where the first stage of the guidance law could produce a set of steering angles resulting in a cone angle very close to 90°. The thrust produced in such a situation would be extremely small, and result in less progress being made compared to if the guidance law accepted a thrust direction which does not point exactly towards the local optimum. By accepting a non-ideal direction, the spacecraft can still make progress towards its goal.

3.4.2 Formulation

The ideal steering angles α^*, β^* are used to compute an idealized cone angle.

$$\varphi^* = \arccos(\hat{u}_i \cdot \hat{n}^*) \tag{3.11}$$

where $\hat{n}^* = \hat{n}(\alpha^*, \beta^*)$ can be computed using (3.1) and $\hat{u}_i = -\frac{\vec{r}_\odot}{||\vec{r}_\odot||}$. Both vectors are expressed in the same frame for computational procedures (e.g. the LVLH frame).

φ^* is compared between two angle thresholds:

1. **Feathering Threshold**: κ_f
2. **Degraded Operation Threshold**: κ_d

Consider a vector $\hat{b}$ which is normal to both $\hat{u}_i$ and $\hat{n}^*$. For example, $\hat{b} = \hat{u}_i \times (\hat{n}^* \times \hat{u}_i)$.

The resulting sail normal $\hat{n}$ is then calculated as:

$$\hat{n} = \begin{cases} \hat{n}^* & \cos\varphi^* > \cos\kappa_d \\ \cos\kappa_d\ \hat{u}_i + \sin\kappa_d\ \hat{b} & \cos\varphi^* \in [\cos\kappa_f, \cos\kappa_d] \\ \hat{b} & \cos\varphi^* < \cos\kappa_f \end{cases} \tag{3.12}$$

The 3 cases in Equation 3.12 correspond to **nominal, degraded, and feathered** operation.

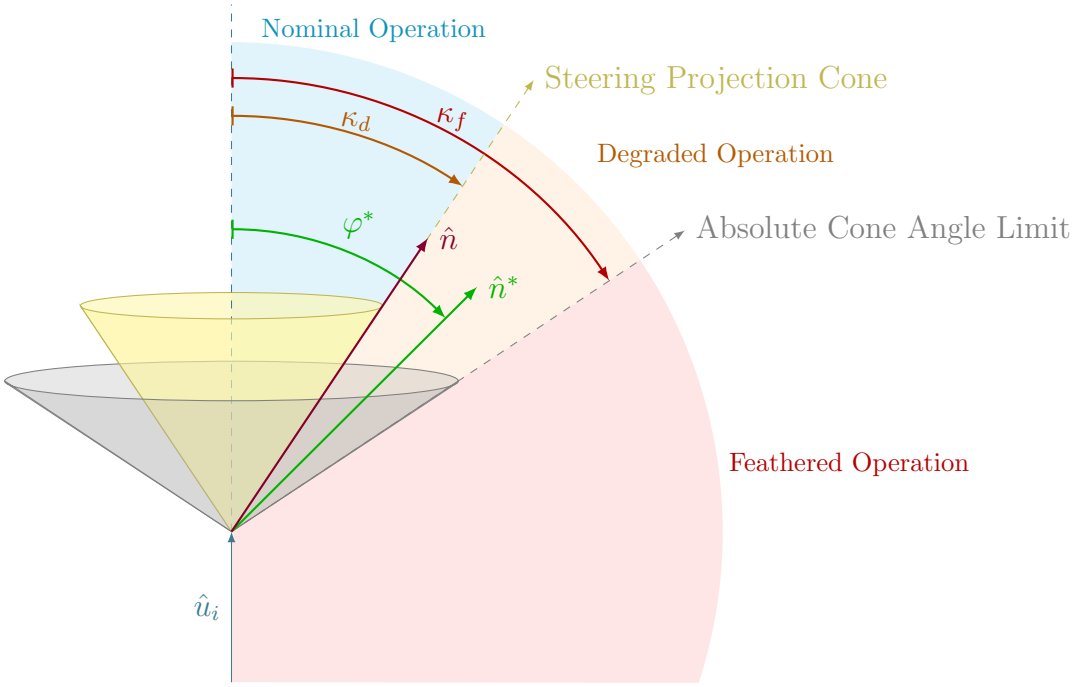

Figure 3.4: Overview of steering angle regularization heuristic. Note that this diagram is not taken relative to any specific coordinate system, but rather aligned with the direction of incident sunlight as the vertical.

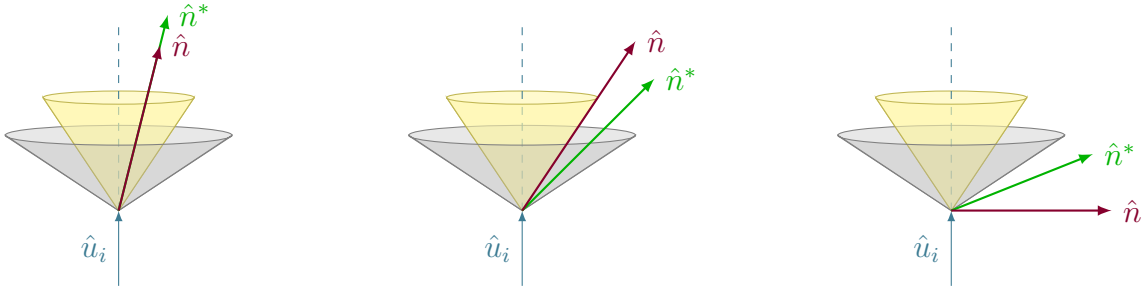

(a) Nominal operations; $\hat{n}$ is equal to $\hat{n}^*$.

(b) Degraded operations; $\hat{n}^*$ is projected onto the yellow cone.

(c) Feathered operations; $\hat{n}$ is normal to $\hat{u}_i$.

Figure 3.5: Three different cases of the steering heuristic illustrated.

Figures 3.4 and 3.5 give an overview of the steering angle heuristic, as well as a visual depiction of each case.

The most interesting case to discuss is the degraded operation mode. The resultant direction of $\hat{n}$ is equivalent to projecting $\hat{n}^*$ upon the cone formed at an angle of κ_f relative to $\hat{u}_i$.

The feathering threshold κ_f can be set based on the maximum achievable angle for a solar sail, while the degraded operation threshold κ_d can be set to an even lower angle to enforce greater production of thrust. These parameters are completely agnostic to the solar sail thrust model used, and could readily be extended to a variety of spacecraft configurations.

3.4.3 Assembly of Output

Following the computation of (α^*, β^*) by the first stage of the algorithm, φ^* is computed using Equation 3.11. $\hat{n}^*$ is computed in referential form (i.e. its components are calculated relative to some reference frame), and the vector $\hat{b}$ is formed. Then, Equation 3.12 is used to calculate $\hat{n}$, using conditional expressions.

Expressing $\hat{n}$ in $\vec{\mathcal{F}}_{\text{LVLH}}$, the steering angles α and β can be found by working backwards from Equation 3.1. A reference formulation is given below:

$$\alpha = \text{atan2}\left(\hat{n} \cdot \hat{x}_{\text{LVLH}},\ \hat{n} \cdot \hat{y}_{\text{LVLH}}\right)$$
$$\beta = \text{atan2}\left(\hat{n} \cdot \hat{z}_{\text{LVLH}},\ \sqrt{(\hat{n} \cdot \hat{x}_{\text{LVLH}})^2 + (\hat{n} \cdot \hat{y}_{\text{LVLH}})^2)}\right)$$

3.5 Implementation in Simulation

With reference to the architecture in Figure 3.3 and the procedures shown above, the complete guidance law and dynamics are implemented in two separate simulators.

Simulation is used to obtain trajectories through the solution of the planetocentric solar sail feedback guidance problem. Several cases of the guidance problem are solved, and the resultant trajectories are then analyzed.

3.5.1 MATLAB Implementation

Link to GitHub Repository

The MATLAB implementation, named "SLyGA" (Solar Lyapunov Guidance Algorithm) is the more fully featured simulator of the pair. SLyGA includes diagnostic metrics and plotting utilties to generate visualizations of trajectories.

MATLAB's built-in ODE integrators are mature and well-tested, and therefore SLyGA is used for high-fidelity simulation cases.

A key drawback of this implementation is its speed – simulation runs take anywhere from tens of seconds to several minutes to complete. This makes it unsuitable for optimization of the guidance law.

3.5.2 C/Python Implementation

Link to GitHub Repository

The C/Python implementation, named "cshanty" (i.e. Sea Shanty) is built for tuning the weights of the guidance law. The C portion of the codebase contains all of the guidance law and dynamics, as well as a custom ODE integrator based on weights found by Verner [33]. The Python portion of the code wraps the C simulator into an interface for optimization using SciPy [34].

3.5.3 Trajectory Cases

Table 3.2 gives four trajectory cases used to assess the performance of the guidance law.

Case		p $[1 \times 10^3\,\mathrm{m}]$	f	g	h	k	L [rad]
GEO Disposal	Initial	42164	0	0	0	0	0
	Final	42464	0	0	Free	Free	N/A
Plane Change	Initial	20000	0.5	0	1	0	0
	Final	20000	0.5	0	-1	0	N/A
"Benchmark"	Initial	20 000	0.5	−0.2	0.5	0	0
	Final	25 000	0.2	0.5	0	0.3	N/A
Polar GSO	Initial	11625	0.725	0	0	0	0
	Final	42165	0	0	0	-1	N/A

Table 3.2: Trajectory cases.

Free orbital elements are implemented by assigning a value of zero to the corresponding weight (i.e. $W_{\text{œ}} = 0$).

For each trajectory case, values of the guidance parameters used are presented in Table 3.3.

Case	W_P	γ	$r_{p,\min}$	W_p	W_f	W_g	W_h	W_k	κ_d	κ_f
GEO Disposal	0	N/A	N/A	5	0.5	1	0	0	70°	91°
Plane Change	1	1	10 000 km	1	1	1	1	1	70°	91°
"Benchmark"	0	N/A	N/A	1	1	1	1	1	70°	91°
Polar GSO	1	5	6878 km	1	1	1	1	1	70°	91°

Table 3.3: Guidance parameters for each case.

3.6 Tuning of Guidance Algorithm

The parameters in Table 3.3 are a baseline obtained from manual tuning. Optimization is performed to find the parameters yielding minimum time-of-flight.

3.6.1 Sail Angle Heuristic Tuning

Keeping κ_f fixed, the value of κ_d is optimized using bounded univariate optimization through measured time-of-flight in the Benchmark case. The value of κ_d in the interval $[30°, 85°]$ is determined using Brent's method [35].

The resultant optimum of $\kappa_d \approx 64°$ is used for proceeding analysis of all the other cases. Note that this is not an exact optimum for all of the other cases, and further tuning is to be done on a case-by-case basis.

3.6.2 Orbital Element Weight Tuning

All five weights $W_{\text{œ}}$, $\text{œ} \in \{p, f, g, h, k\}$ are optimized using a simulated-annealing global optimization algorithm. The computationally efficient implementation of the simulation in C allows for the global optimization runs to perform thousands of iterations in under one hour.

Chapter 4

Results and Discussion

This chapter discusses the outcomes of each trajectory case, in the context of guidance law performance. Consideration of the methodology is used to explain some of the observed behaviours, and deficiencies are noted for improvement.

4.1 Baseline Case Runs

This section covers the baseline trajectory cases outlines in Tables 3.2 and 3.3.

Table 4.1 summarizes the outcomes of each case. Discussion proceeds.

Case	Convergence Tolerance	Time of Flight (d)	Number of Revolutions	Δv Expenditure (m/s)
GEO Disposal	0.005	62.44	62	13.1
Plane Change	0.005	1020	1944	13570.3
"Benchmark"	0.005	610	858	6673.2
Polar GSO	0.03	490	494	9686.7

Table 4.1: Summary of outcomes for each case.

Overall, it is evident that despite being convergent, the guidance law is extremely slow in bringing the spacecraft to the target orbit.

The low thrust produced by the sail is not the key issue; rather, it is the lack of availability of thrust in a given direction. For example, a continuous thrust plane change maneuver

involves continuously changing the direction of applied thrust. The direction desired by the first stage of the guidance law is not always available, and the solar sail often ends up being feathered (this effect has not yet been quantified; pending measurement of time spent in degraded/feathered operational mode).

Part of the issue with the long time of flight is the convergence tolerance (measured as the sum of the squares of the error in each element, weighed by W_{∞}; this will be changed to the value of Q in the future). The guidance law can reach an error of about 0.05 reasonably quickly, but spends a substantial amount of time finely correcting its trajectory at the end, resulting in very slow convergence to the final threshold.

For initial orbits very close to the target orbit (e.g. GEO disposal case), the guidance law struggles with closing the gap, and often results in extremely long missions. Altering guidance weights helps with this somewhat (see the guidance weights of the GEO disposal case, for example), but it is currently unknown whether there are also numerical artifacts to consider.

More insights are evident through inspection of the plots of the trajectory and orbital elements. Discussion on these is presented in the next section.

4.2 Global Optimization Runs

Global weight optimization was performed for the latter two baseline cases. The optimized guidance law tunings are compared against their unoptimized counterparts in Table 4.2.

Case	Time of Flight (d)	Number of Revolutions	Δv Expenditure (m/s)
"Benchmark", baseline	610	858	6673.2
"Benchmark", optimized	388	622	6193.0
Polar GSO, baseline	490	494	9686.7
Polar GSO, optimized	375	323	8352.0

Table 4.2: Comparison of optimized cases against their baselines.

The two cases still use their original convergence tolerances in the optimized tunings.

Plots of the trajectories and orbital elements are shown in Sections 4.2.1 and 4.2.2.

4.2.1 Benchmark Case

Baseline $W_{\text{œ}}$: $\{1, 1, 1, 1, 1\}$

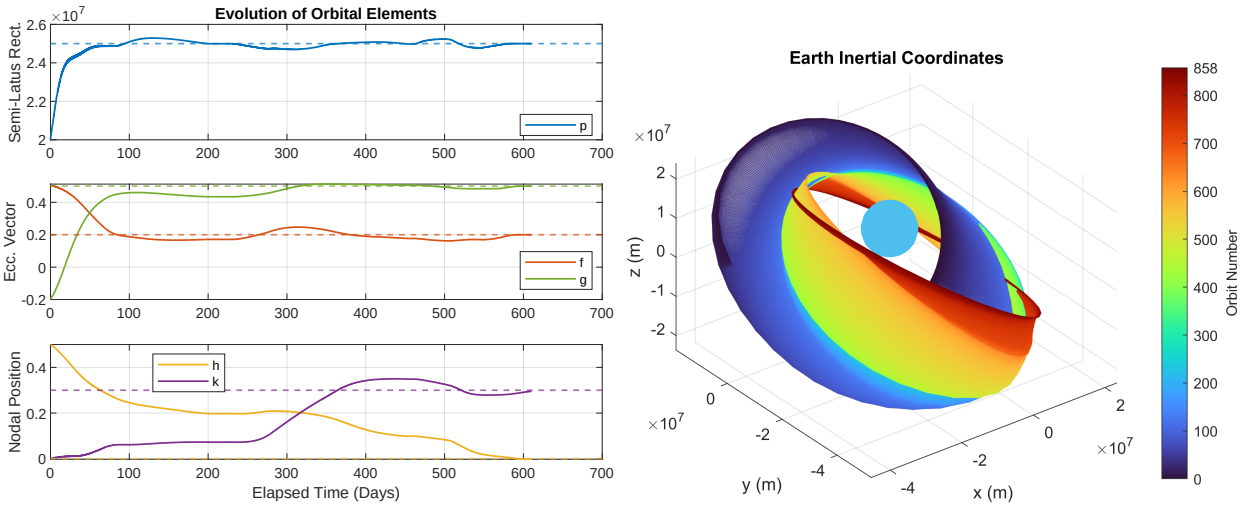

(a) Evolution of orbit elements in time. (b) Trajectory plot.

Figure 4.1: Benchmark transfer case, baseline.

Optimal $W_{\text{œ}}$: $\{1.774, 0.5149, 0.3327, 9.925, 0.5317\}$

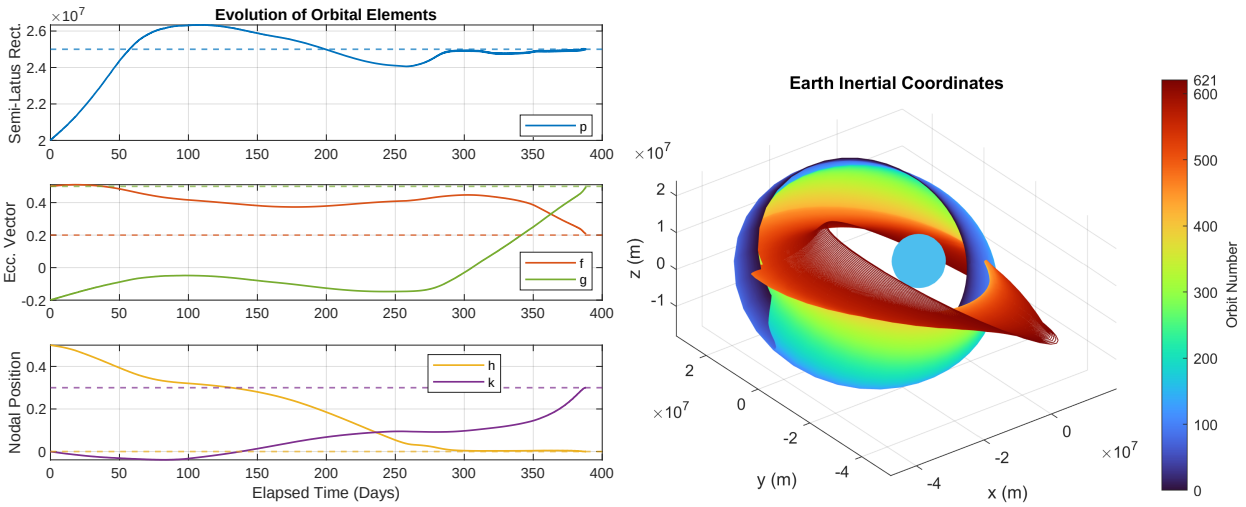

(a) Evolution of orbit elements in time. (b) Trajectory plot.

Figure 4.2: Benchmark transfer case, optimal tuning.

4.2.2 Polar GSO Case

Baseline $W_{\text{œ}}$: $\{1, 1, 1, 1, 1\}$

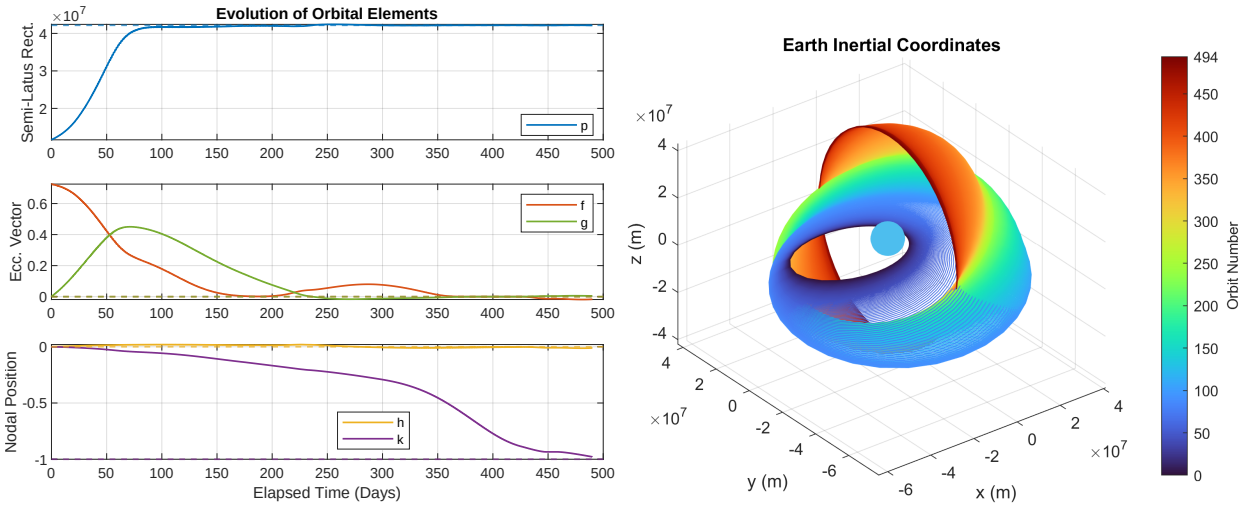

(a) Evolution of orbit elements in time. (b) Trajectory plot.

Figure 4.3: GTO to polar transfer, baseline.

Optimal $W_{\text{œ}}$: $\{8.959, 2.132, 1.722, 3.559, 9.789\}$

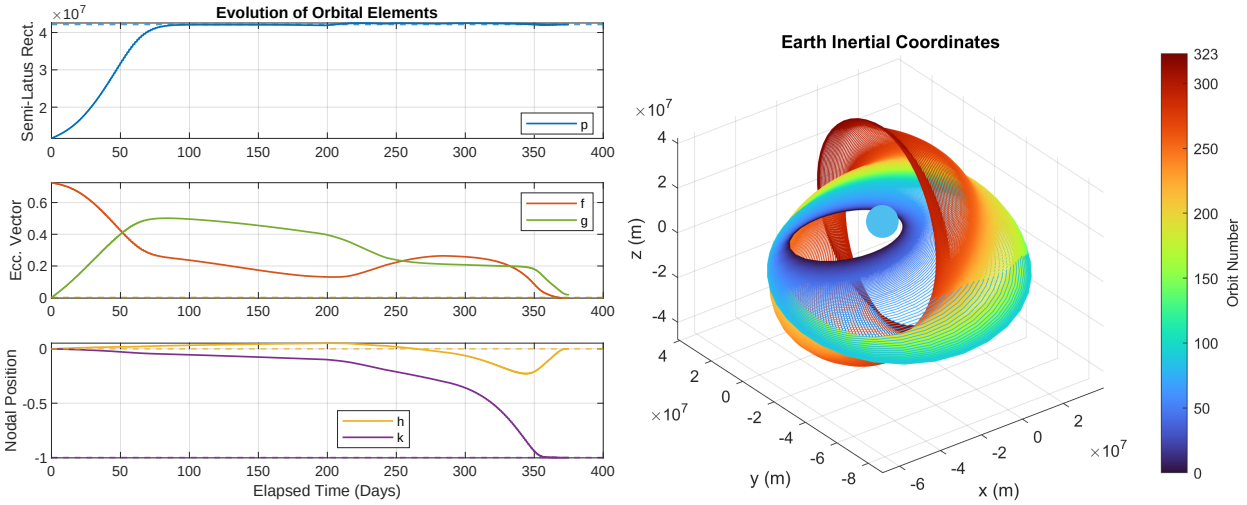

(a) Evolution of orbit elements in time. (b) Trajectory plot.

Figure 4.4: GTO to polar transfer, optimal tuning.

Note: animated versions of the trajectory plots can be found on this webpage.

4.2.3 Discussion

The improvement in time-of-flight (and number of revolutions) is remarkable. By inspecting the plots of the orbital elements, it is clear that adjusting the weights of the guidance changes the "strategy" employed by the guidance law.

By emphasizing certain elements over others, the guidance law is more willing to accept an increase in error in one element for a reduction in another. This is exemplified in Figure 4.2a.

By inspecting the trajectory plots, it is evident that the optimized transfers "waste fewer actions" compared to their baseline counterparts. In the Benchmark case, the total Δv expenditures are very similar, but the trajectory taken by the optimized tuning looks far more direct than the baseline case.

Chapter 5

Future Work

Next steps are identified for work on the guidance law, and a development timeline is presented.

5.1 Further Development of the Guidance Law

Subsequent work for the guidance law is divided into two sections:

1. Refining the guidance law for better performance. For example, determining the limits of what the guidance law can handle before it becomes non-convergent.
2. Subjecting the guidance law to new system dynamics. For example, applying the guidance law to spacecraft in Venus orbit instead of Earth, or even heliocentric orbits.

Both pathways are considered, and are to be worked on in parallel.

5.1.1 Performance Improvements and Characterization

Although the basic structure of the guidance law has been established, there are many possibilities for tuning the guidance law and revising its structure to improve performance under challenging conditions. Increasing the number of cases simulated is a good overall target for motivating immediate next steps.

Feature Completion

The first step in continuing to simulate trajectory cases is to ensure that the numerical implementations of the project are feature-complete.

Notably missing from the work done so far is a thorough test of the the penalty function. There are currently issues with the numerical implementation which must be debugged.

Convergence Studies

Determining limits on convergence of a feedback guidance law is challenging, but there may be value in sweeping large swaths of the parameter space to determine if guidance law works better for certain cases. Of key interest are orbits which are very closer to each other, such as for the GEO disposal case.

Figuring the issues with "last-mile" convergence would mark a significant improvement. A helpful approach in doing so may be to study the evolution of Q in time, alongside plots of the orbital elements. As mentioned in Section 4.2.3, a quantitative analysis of how often the sail operates in degraded or feathered mode could provide opportunities for improving the approach taken to regularize the steering angles.

Steering Angle Regularization Heuristic Rework

The current approach for steering angle regularization is simple and functional, but lacks a solid mathematical justification in its design. Designing a regularization scheme which is based on some form of mathematical optimality is desirable from a point of analysis, and may lead to better performance.

Coverstone [5] presents a feedback guidance law which maximizes the amount of thrust generated by a solar sail towards a given direction. Oguri [12] makes use of a similar approach. The idea is to find some $\hat{n} = \hat{n}^\dagger$ such that the product $\vec{F}(\hat{n}) \cdot \hat{n}^*$ (i.e. the projection of the resultant acceleration upon the ideal steering direction) is maximized. This can yield an orientation which is neither exactly on the "projection cone" nor directly facing towards $\hat{n}^*$, but which actually maximizes the "amount of progress" made towards the ideal direction.

Optimization

Further optimization runs can be performed using the current implementation, and improved once the above changes are made.

Exploring a large variety of transfer cases may allow the discovery of trends in optimal weights (e.g. emphasizing W_p when orbit raising is needed), such that a general heuristic can be created for tuning guidance weights in the absence of a simulator.

5.1.2 Applications to New Dynamics

The current dynamics model is very simple. Demonstration of robustness to plant model variation would be a very attractive attribute for the guidance law.

Orbital Perturbations

The addition of zonal and tesseral gravitational effects is a straightforward addition to the dynamics model which much more faithfully represents spacecraft orbits around Earth.

Adding gravity from the Sun and Moon is also relatively straightforward.

Other Bodies

Only Earth-centric orbits have been considered so far. With increasing interest in cislunar space, it may be useful to investigate the applicablity of solar sails for translunar trajectories.

There are also mission using solar sails to the inner solar system, such as a Mercury sample return mission proposed by Hughes [36]. Although the guidance law developed in this project is targeted at planetocentric orbits, it may also work for heliocentric trajectories.

Sail Thrust Models

So far, only a flat idealized sail has been considered. Ref. [12] uses a more sophisticated thrust model incorporated into the *Q-Law*. It would be interesting to see how the guidance law produced in this project compares against Oguri's.

5.2 Far Future Ideas

These ideas are unsuitable for investigation in the scope of a thesis, but would be interesting for further work beyond the scope of this project.

Non-Keplerian Orbits

Solar sails are a prime candidate for exploiting non-Keplerian trajectories such as halo orbits around Lagrange points; the lack of a propellant consumption leads to an uncapped mission life in a frozen orbit. Applying the guidance law to a multibody problem could give interesting results, but is made difficult by the lack of orbital elements to describe such trajectories.

As a Starting Point for Global Methods

The trajectories produced by the guidance law could be used as an initial guess for global methods to kickstart their optimization processes.

5.3 Timeline

The development timeline proceeeding the interim report is shown below in Figure 5.1, starting the week of January 8, 2024.

Figure 5.1: Timeline for ESC499 in winter semester, post-interim report.

References

[1] Dan Lev, Roger M Myers, Kristina M Lemmer, Jonathan Kolbeck, Hiroyuki Koizumi, and Kurt Polzin, "The Technological and Commercial Expansion of Electric Propulsion," *Acta Astronautica*, Vol. 159, pp. 213–227, 2019.

[2] David A Spencer, Bruce Betts, John M Bellardo, Alex Diaz, Barbara Plante, and Justin R Mansell, "The Lightsail 2 Solar Sailing Technology Demonstration," *Advances in Space Research*, Vol. 67, No. 9, pp. 2878–2889, 2021.

[3] Osamu Mori, Hirotaka Sawada, Ryu Funase, Mutsuko Morimoto, Tatsuya Endo, Takayuki Yamamoto, Yuichi Tsuda, Yasuhiro Kawakatsu, Jun'ichiro Kawaguchi, Yasuyuki Miyazaki, *et al.*, "First Solar Power Sail Demonstration by IKAROS," *Transactions of the Japan Society for Aeronautical and Space Sciences, Aerospace Technology Japan*, Vol. 8, No. ists27, pp. 425–431, 2010.

[4] Paul D Fieseler, "A Method for Solar Sailing in a Low Earth Orbit," *Acta Astronautica*, Vol. 43, No. 9-10, pp. 531–541, 1998.

[5] Victoria L Coverstone and John E Prussing, "Technique for Escape from Geosynchronous Transfer Orbit Using a Solar Sail," *Journal of Guidance, Control, and Dynamics*, Vol. 26, No. 4, pp. 628–634, 2003.

[6] V Lappas, S Pellegrino, H Guenat, M Straubel, H Steyn, V Kostopoulos, E Sarris, O Takinalp, S Wokes, and A Bonnema, "DEORBITSAIL: De-orbiting of Satellites Using Solar Sails," in *2011 2nd International Conference on Space Technology*, IEEE, 2011, pp. 1–3.

[7] Colin R McInnes, *Solar Sailing: Technology, Dynamics and Mission Applications*. Springer Science & Business Media, 2004.

[8] Marc R Ilgen, "Low Thrust OTV Guidance Using Liapunov Optimal Feedback Control Techniques," *Astrodynamics 1993*, pp. 1527–1545, 1994.

[9] Anastassios Petropoulos, "Low-thrust Orbit Transfers Using Candidate Lyapunov Functions with a Mechanism for Coasting," in *AIAA/AAS Astrodynamics Specialist Conference and Exhibit*, 2004, p. 5089.

[10] Gábor Varga and José Manuel Sánchez Pérez, "Many-revolution Low-thrust Orbit Transfer Computation Using Equinoctial Q-Law Including J2 and Eclipse Effects," *Advances in the Astronautical Sciences*, Vol. 156, pp. 2463–2481, 2016.

[11] Sanjeev Narayanaswamy and Christopher J. Damaren, "Equinoctial Lyapunov Control Law for Low-thrust Rendezvous," en, *Journal of Guidance, Control, and Dynamics*, Vol. 46, No. 4, pp. 781–795, Apr. 2023.

[12] Kenshiro Oguri, Gregory Lantoine, Anastassios E Petropoulos, and Jay W McMahon, "Solar Sailing Q-law for Planetocentric, Many-revolution Sail Orbit Transfers," *Journal of Guidance, Control, and Dynamics*, pp. 1–10, 2023.

[13] CH Yam, DD Lorenzo, and D Izzo, "Low-thrust Trajectory Design as a Constrained Global Optimization Problem," *Proceedings of the Institution of Mechanical Engineers, Part G: Journal of Aerospace Engineering*, Vol. 225, No. 11, pp. 1243–1251, 2011.

[14] Christopher Damaren, Anton H. J. De Ruiter, and James R Forbes, *Spacecraft Dynamics and Control: An Introduction*, 1st ed. Wiley, 2013.

[15] Michael JH Walker, B Ireland, and Joyce Owens, "A Set of Modified Equinoctial Orbit Elements," *Celestial mechanics*, Vol. 36, No. 4, pp. 409–419, 1985.

[16] Gooding Universal Elements, 2021.

[17] David Morante, Manuel Sanjurjo Rivo, and Manuel Soler, "A Survey on Low-thrust Trajectory Optimization Approaches," *Aerospace*, Vol. 8, No. 3, p. 88, 2021.

[18] Matthew P Kelly, "Transcription Methods for Trajectory Optimization," *Tutorial, Cornell University, Feb*, p. 21, 2015.

[19] Jon A Sims and Steve N Flanagan, "Preliminary Design of Low-thrust Interplanetary Missions," 1997.

[20] Fariba Fahroo and I Michael Ross, "Direct Trajectory Optimization by a Chebyshev Pseudospectral Method," *Journal of Guidance, Control, and Dynamics*, Vol. 25, No. 1, pp. 160–166, 2002.

[21] Sanjeev Narayanaswamy and Christopher J Damaren, "Comparison of the Legendre–Gauss Pseudospectral and Hermite–Legendre–Gauss–Lobatto Methods for Low-thrust Spacecraft Trajectory Optimization," *Aerospace Systems*, Vol. 3, No. 1, pp. 53–70, 2020.

[22] Bo James Naasz, "Classical Element Feedback Control for Spacecraft Orbital Maneuvers," Ph.D. Dissertation, Virginia Tech, 2002.

[23] Mirue Choi and Christopher J Damaren, "Structural Dynamics and Attitude Control of a Solar Sail Using Tip Vanes," *Journal of Spacecraft and Rockets*, Vol. 52, No. 6, pp. 1665–1679, 2015.

[24] Elena Polyakhova and Vladimir Korolev, "The Solar Sail: Current State of the Problem," in *AIP Conference Proceedings*, Vol. 1959, 1, AIP Publishing, 2018.

[25] Hiraku Sakamoto, KC Park, and Yasuyuki Miyazaki, "Effect of Static and Dynamic Solar Sail Deformation on Center of Pressure and Thrust Forces," in *AIAA Guidance, Navigation, and Control Conference and Exhibit*, 2006, p. 6184.

[26] Leonard Felicetti, Matteo Ceriotti, and Patrick Harkness, "Attitude Stability and Altitude Control of a Variable-geometry Earth-orbiting Solar Sail," *Journal of Guidance, Control, and Dynamics*, Vol. 39, No. 9, pp. 2112–2126, 2016.

[27] Yuichi Tsuda, Osamu Mori, Ryu Funase, Hirotaka Sawada, Takayuki Yamamoto, Takanao Saiki, Tatsuya Endo, Katsuhide Yonekura, Hirokazu Hoshino, and Jun'ichiro Kawaguchi, "Achievement of Ikaros—japanese Deep Space Solar Sail Demonstration Mission," *Acta Astronautica*, Vol. 82, No. 2, pp. 183–188, 2013.

[28] Les Johnson, Roy Young, Edward Montgomery, and Dean Alhorn, "Status of Solar Sail Technology Within NASA," *Advances in Space Research*, Vol. 48, No. 11, pp. 1687–1694, 2011.

[29] Leonel Rios-Reyes and Daniel J Scheeres, "Generalized Model for Solar Sails," *Journal of Spacecraft and Rockets*, Vol. 42, No. 1, pp. 182–185, 2005.

[30] Yuichi Tsuda, Takanao Saiki, Ryu Funase, and Yuya Mimasu, "Generalized Attitude Model for Spinning Solar Sail Spacecraft," *Journal of Guidance, Control, and Dynamics*, Vol. 36, No. 4, pp. 967–974, 2013.

[31] Lester L Sackett, "Optimal Solar Sail Planetocentric Trajectories," 1977.

[32] Malcolm Macdonald and Colin R McInnes, "Analytical Control Laws for Planet-centered Solar Sailing," *Journal of Guidance, Control, and Dynamics*, Vol. 28, No. 5, pp. 1038–1048, 2005.

[33] James H Verner, "Numerically Optimal Runge–kutta Pairs with Interpolants," *Numerical Algorithms*, Vol. 53, No. 2-3, pp. 383–396, 2010.

[34] Pauli Virtanen, Ralf Gommers, Travis E. Oliphant, Matt Haberland, Tyler Reddy, David Cournapeau, Evgeni Burovski, Pearu Peterson, Warren Weckesser, Jonathan Bright, Stéfan J. van der Walt, Matthew Brett, Joshua Wilson, K. Jarrod Millman, Nikolay Mayorov, Andrew R. J. Nelson, Eric Jones, Robert Kern, Eric Larson, C J Carey, İlhan Polat, Yu Feng, Eric W. Moore, Jake VanderPlas, Denis Laxalde, Josef Perktold, Robert Cimrman, Ian Henriksen, E. A. Quintero, Charles R. Harris, Anne M. Archibald, Antônio H. Ribeiro, Fabian Pedregosa, Paul van Mulbregt, and SciPy 1.0 Contributors, "SciPy 1.0: Fundamental Algorithms for Scientific Computing in Python," *Nature Methods*, Vol. 17, pp. 261–272, 2020.

[35] Richard P Brent, *Algorithms for Minimization Without Derivatives*. Courier Corporation, 2013.

[36] Gareth W Hughes, Malcolm Macdonald, Colin R McInnes, Alessandro Atzei, and Peter Falkner, "Sample Return from Mercury and Other Terrestrial Planets Using Solar Sail Propulsion," *Journal of spacecraft and rockets*, Vol. 43, No. 4, pp. 828–835, 2006.